

GT2011-4) %d*

INVESTIGATION OF THE TIP CLEARANCE FLOW IN A COMPRESSOR CASCADE USING A NOVEL LASER MEASUREMENT TECHNIQUE WITH HIGH TEMPORAL RESOLUTION

Andreas Fischer

Technische Universität Dresden
Laboratory of Measurement and
Testing Techniques
D-01062 Dresden, Germany
andreas.fischer2@tu-dresden.de

Lars Büttner

Technische Universität Dresden
Laboratory of Measurement and
Testing Techniques
D-01062 Dresden, Germany
lars.buettner@tu-dresden.de

Jürgen Czarske

Technische Universität Dresden
Laboratory of Measurement and
Testing Techniques
D-01062 Dresden, Germany
juergen.czarske@tu-dresden.de

Marcel Gottschall

Technische Universität Dresden
Institute of Fluid Mechanics
D-01062 Dresden, Germany
marcel.gottschall@tu-dresden.de

Ronald Mailach

Technische Universität Dresden
Institute of Fluid Mechanics
D-01062 Dresden, Germany
ronald.mailach@tu-dresden.de

Konrad Vogeler

Technische Universität Dresden
Institute of Fluid Mechanics
D-01062 Dresden, Germany
konrad.vogeler@tu-dresden.de

ABSTRACT

The understanding of the tip clearance flow in axial compressors is a key issue for developing new compressors with enhanced efficiency and reduced noise for instance. However, necessary flow measurements in the blade tip region and within the tip clearance are challenging due to the small gap width. The application of a novel optical measurement technique named Doppler global velocimetry with laser frequency modulation is presented, which provides velocity field measurements of all three velocity components non-intrusively in the tip clearance flow of a linear cascade at near stall conditions. These array measurements have a high temporal resolution enabling turbulence analysis such as the evaluation of velocity standard deviations and turbulence spectra up to several kilohertz. Conventional pneumatic and hot-wire measurements in planes at the inlet and the outlet as well as on the blade surface were taken to complete the flow pattern and validate the data of the Doppler global velocimetry.

Wake measurements identified a strong flow separation in the rear suction side dominating the transient character of the cascade flow. Towards the endwall this high loss region is reduced by the clearance flow and the resulting vortex, which is obviously not affected by the profile separation and the

pulsating blockage frequency. Inside the blade passage and the tip clearance the Doppler global velocimetry measurements allowed a spatial assignment of the origin of the tip leakage flow and the downstream developing vortex. In addition, the tip clearance vortex could be resolved and identified successfully as the most dominant turbulence generating effect in the near endwall region at this high loading operating point of the blading.

Keywords: compressor cascade, tip leakage flow, velocity field measurement, unsteady flow, turbulence analysis

NOMENCLATURE

Symbols

α_1, α_2	[deg]	inlet and outlet flow angle
$\Delta\alpha$	[deg]	blade turning
λ	[deg]	stagger angle
σ_v	[m/s]	velocity standard deviation (uncertainty)
ζ	[-]	total pressure loss
c	[m/s]	flow velocity
$c_{k,RMS}$	[m/s]	standard deviation of velocity component k

c_x, c_y, c_z	[m/s]	flow velocity components
c_L	[m/s]	light speed
f_c	[Hz]	laser centre frequency
f_D	[Hz]	Doppler frequency
h	[m]	blade height
\vec{i}	[-]	laser incident direction
l	[m]	chord
l_x	[m]	axial cascade width
Ma	[-]	Mach number
\vec{o}	[-]	observation direction
p_t	[Pa]	total pressure
P_s	[W]	scattered light power
Re	[-]	Reynolds number
s	[m]	tip clearance width
SVO	[-]	streamwise vorticity
t	[m]	pitch
T	[s]	temporal resolution
x, y, z	[m]	axial, circumferential and radial coordinate

Acronyms

DGV	Doppler Global Velocimetry
FM	Frequency Modulation
HWA	Hot-Wire Anemometry
LDA	Laser Doppler Anemometry
PIV	Particle Image Velocimetry
PS	Pressure Side
PSD	Power Spectrum Density
SS	Suction Side
TCV	Tip Clearance Vortex
5HP	5-Hole-Probe

1 INTRODUCTION

A primary goal of jet engine development is to increase the pressure ratio and to enhance the efficiency, while reducing the number of blades and stages. It is one of the design challenges to include beneficial unsteady flow effects and to account for secondary flows to improve the engine parameters. This requires a detailed physical understanding of the time-resolved three dimensional flow pattern and the resulting effects on performance and aerodynamic stability.

In modern compressors with high aerodynamic quality the tip leakage flow is of crucial importance for loss production and pressure rise due to the blockage effect in the endwall region (Wisler [1]). Considering the flow stability, the tip leakage flow plays an important role on the rotating stall inception process (Hoying et al. [2], Mailach et al. [3], Vo et al. [4]) for instance.

The flow field in the tip region of cantilevered stator vane rows and rotor blade rows is dominated by the tip clearance vortex (TCV), which is illustrated in fig. 1. The pressure difference of the blade drives a balancing out clearance flow through this gap from the pressure side (PS) toward the suction side (SS). When the jetlike tip leakage flow enters the next blade passage, it interacts with the main flow and other secondary flow phenomena such as the passage vortex and rolls up into a spiral vortex. Chen et al. [5] and Storer and Cumpsty

[6] considered the leakage flow and the main flow as separate mass flows and the vortex trajectory is therefore determined by the momentum ratio of the tip leakage flow and the main passage flow. At the upstream boundary of the TCV, the tip leakage flow interacts with the incoming main flow. As a result, a blockage zone is formed near the wall and the incoming flow is partly diverted toward the hub or casing.

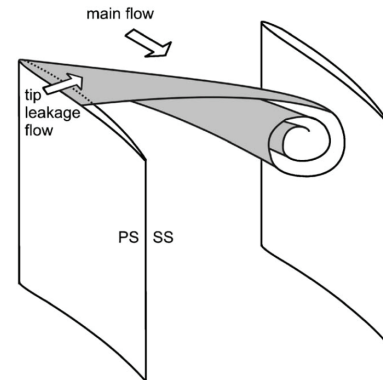


Figure 1. Flow structure of the tip clearance vortex in an axial compressor blade row

The characteristics of the TCV depend on various geometrical and aerodynamical parameters. As discussed by Lakshminarayana et al. [7] and Tan [8], the tip clearance height, Reynolds and Mach number, blade thickness and loading, the machine configuration (rotor alone, single or multistage compressor...), but also the inlet flow turbulence, the casing wall boundary layer and others play an important role on the formation of the TCV and the potential interaction among adjacent vortices and the passage flow.

Numerical simulations are not able to capture all details of the complex flow field in the endwall region with sufficient accuracy and acceptable computing times yet. Therefore, to enhance the physical understanding, measurements in the blade tip region and within the tip clearance are necessary. Especially the latter is challenging due to the small tip gap dimensions. Flow measurements using pressure probes are possible [9], but intrusive. The same is true for hot-wire anemometers (HWA), which is crucial when measuring in the tip gap. For this reason, optical, non-intrusive measurement devices such as Laser Doppler Anemometry (LDA) have been applied in the past.

A number of studies using this technique have achieved additional knowledge on the rotor tip region flow. Murthy and Lakshminarayana [10] and Stauter [11] provide information on the characteristics of the time-averaged rotor blade tip clearance vortex. LDA experiments concerning the convection of wakes through blade rows and within the axial gap can already be found in Hathaway et al. [12], Lehmann et al. [13], and Mailach et al. [14]. LDA analysis in the rotor tip clearance found dominant flow in reverse direction at high clearance levels named “vortex spillover” by several authors, i. e. Mailach [15]. Also Suder and Celestina [16] discussed the passage shock - TCV interaction at design speed as well as the

TCV features at part speed in the absence of shocks. Recently, Michon et al. [17] provide a detailed data base of the 3D flow field of the entire compressor stage for off-design conditions. Other authors like Ma et al. [18] examined the 3D flow field in the rotor blade tip region using a LDA system to characterize the periodical unsteadiness of the rotor TCV, which can appear due to blade row interactions, especially because of the passing wakes.

However, LDA is a point-wise technique. Measurements of flow fields are time-consuming and require periodicity of the flow using phase triggered measurements. Due to this, particle image velocimetry (PIV) is demonstrated to be a useful tool for flow field investigations in turbomachinery by Tisserant and Breugelmann [19] and Balzani et al. [20]. Sanders et al. [21] investigated the time-resolved flow field at midspan for both subsonic and transonic flow conditions. Further experiments in a 1.5-stage large scale compressor using stereoscopic PIV were performed by Liu et al. [22]. These authors showed instantaneous pictures in several cross sections of the rotor blade passage flow field. The time-resolved results indicate the inherent unsteadiness of the TCV which finally breaks down. Furthermore, concerning the technical aspects also PIV measurements were recently conducted by Voges et al. [23] and Wernet et al. [24] in a transonic axial compressor. Measurement errors of 1.7 m/s for the in-plane components and 5.5 m/s for the out-of-plane component were reported. Since multiple measurements with phase synchronization were accomplished, mean and RMS values were measured for a statistical analysis of the flow turbulence. However, velocity spectra are not available because of the low measurement rate. For resolving the three-dimensional unsteady flow structure of the TCV, planar, three componential velocity measurements with high temporal resolution are required. Furthermore, high measurement rates of several kilohertz are desired for calculating turbulence spectra, so that characteristic flow oscillations can be discovered.

The aim of this article is to introduce a novel optical measuring technique for the application in turbomachinery investigations combining the advantages of the previously mentioned non intrusive methods. This Doppler global velocimetry with laser frequency modulation (FM-DGV) [25, 26] provides planar, non-intrusive measurements and high measurement rates up to 100 kHz for all three components. For this purpose, the analysis of the tip clearance flow in a highly loaded linear cascade with an installed clearance width of 5.2 % chord (characteristic for rear high pressure stages and chosen for high tip clearance activity) is presented. The investigation is based on measurement results acquired with FM-DGV and conventional HWA and pressure probes in addition. Here, the investigation is focused on the transient behavior of the tip leakage flow.

2 EXPERIMENTAL METHODS

The approach to the analysis of the tip clearance flow is based on flow measurements in a linear cascade with steady state pressure data as well as time resolved techniques.

2.1 Cascade tunnel and blading

The cascade wind tunnel, schematically shown in fig. 2, operates as a suction channel with a closed measuring section and a radial fan arranged behind the outlet. Thus, a compact design is feasible with a small inlet turbulence intensity of lower than 1%. The pitch t is oriented in a horizontal plane. Different inflow conditions can be arranged by stepwise turning the inlet housing around the measuring chamber. With adjustable tailboards at both inlet and outlet, a homogenous inflow is achievable in almost all operating points. The driving power of 37 kW allows inflow of $Ma = 0.18$ at a measuring section of $380 \times 300 \text{ mm}^2$ (plane 0 in fig. 2).

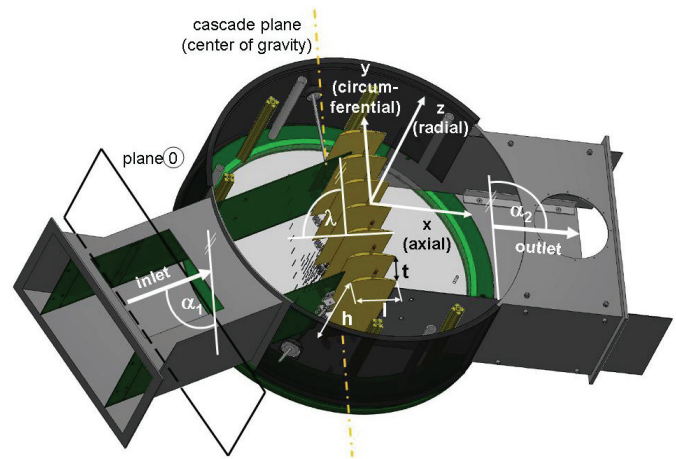


Figure 2. Scheme of cascade tunnel with reference frame

The inlet and outlet flow data were taken at three different positions. The inlet flow reference measurements were obtained using a Prandtl probe (head diameter = 6 mm) was positioned in plane 0 at midspan approximately $8 \cdot t$ upstream the cascade entry. 5-hole-probe (5HP) and hot-wire traversing were carried out at an inflow plane (axial distance of $0.3 \cdot l$ to the leading edge) and an outlet plane (axial distance of $0.05 \cdot l$ behind the trailing edge). The probe traverses cover one pitch around the stagnation streamline of the center vane and the range between midspan and the upper endwall ($z = h$).

During the present investigations the test conditions were characterized by an averaged inlet velocity of 41 m/s which results in an inlet total pressure of approx. 101,272 Pa and an averaged outlet of $Ma = 0.075$.

The linear cascade used in this work consists of seven cylindrical high pressure stator profiles of a front stage of a modern axial compressor. Blades and cascade parameters are scaled from the first stage stator of the four stage low speed research compressor at the Technische Universität Dresden.

The main parameters of the blading and the inflow boundary layer are given in table 1. To amplify the TCV and its interaction with other secondary phenomena, the vanes were not operated at design inflow conditions but with higher incidence, means higher aerodynamic loading of the blading. These near stall conditions correspond to the operation near the

stability limit of the research compressor and are characterized by a 15 deg higher blade turning (compared to the design conditions), high blockage effects at the endwalls and massive leakage flow due to the increased pressure gradient between PS and SS.

inlet flow velocity at plane 0	c_0	41 m/s
Reynolds number	Re	430000
stagger angle	λ	116 deg
inlet flow angle	α_1	22.5 deg
outlet flow angle	α_2	67.7 deg
blade turning angle	$\Delta\alpha$	45 deg
blade height (including gap)	h	300 mm
pitch	t	90.1 mm
chord	l	153.5 mm
tip clearance	s	8 mm
distance measuring plane – endwall		4 mm
displacement thickness		7.2 mm
momentum thickness		6.3 mm

Table 1. Main parameters of the blading

2.2 Measurement technique and data reduction

Besides the conventional techniques the new DGV is described more in detail to assess the systems' capabilities and features regarding the measurement of the tip leakage flow and its application to the linear cascade.

Pressure Probes and HWA

The steady state flow pattern in front and behind the cascade was carried out by traversing a 5HP (head diameter = 2 mm and hole diameter = 0.25 mm) in the y - z planes. The potential measurement error related to the calibrated sensors for this conventional technique is approximately 0.4 K and 2 Pa for temperature and pressure, respectively. Depending on the technique of adjusting the 5HP the uncertainty for the planar flow angle is of approx. 0.2 deg decreasing with higher Re . Beyond that, profile pressure distributions on the vanes' surface were taken. For this purpose the center vane was instrumented at six spanwise positions with 9 pressure tapings at PS and 14 at SS. All measured pressure values are converted to the reference $p_{ref} = 101,325$ Pa to become independent from ambient conditions. Besides the velocity components and total pressure losses (related to the reference measurement at plane 0)

$$\zeta = \frac{P_{t0} - P_t}{P_{t0} - P_0} \quad (1)$$

several secondary flow parameters like helicity, secondary vectors and streamwise vorticity

$$SVO = \frac{\omega_{xy} \cdot l}{c_{inlet}} \quad (2)$$

were analysed to identify the vortex activity. The proportion ω_{xy} of the local vorticity vector into the direction of the corresponding velocity vector at midspan is a result only of

flow components perpendicular to the 2D main flow field (made dimensionless with chord and inflow velocity to compare with other configurations). Therefore it is appropriate to visualize secondary flow related to the almost invariant flow of an infinite cascade without endwall effects.

For measuring the transient flow character a single sensor hot-wire probe was traversed in that planes as well. The system from Dantec Ltd. was used in combination with a probe of a 5 μ m platinum-plated tungsten wire and a thermistor based temperature probe to correct the anemometry data. The sampling rate of 15 kHz and the measurement time of 8.7 s allow a frequency resolution of 0.11 Hz for each measuring point. Selected points were measured over a 35 s period in order to detect possible low frequency disturbances. With the common Fast-Fourier-Transformation one-sided Power Spectral Densities (PSD) of the velocity were determined.

FM-DGV

The Doppler global velocimetry with laser frequency modulation (FM-DGV) was applied to measure the flow in the tip clearance region, because it is an optical, non-intrusive measurement technique [27]. The measurement plane is parallel to the blade tips at the height of $0.987 \cdot h$ (0.5 s from the blade tips). The measurement principle relies on measuring the Doppler frequency shift of laser light, which is scattered on tracer particles in the flow. The general FM-DGV setup is illustrated in fig. 3. The illuminated flow region is observed by a detector array through a molecular absorption cell, which serves as a light frequency to light intensity converter. Since the transmission curve of the absorption cell is non-linear and a sinusoidal laser frequency modulation is applied, the frequency shift information can be mapped by evaluating the ratio of the first and the second harmonic amplitude of the detector signals. Due to the evaluation of the amplitude ratio, the unknown scattered light power is implicitly canceled, which is contrary to conventional DGV systems. For a detailed description of the FM-DGV measurement principle and the system components, it is referred to [25,26,27].

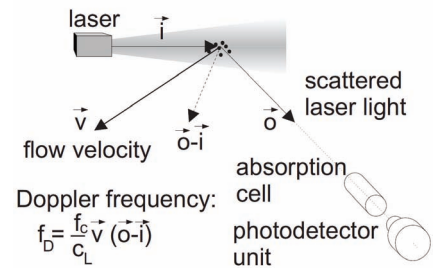


Figure 3. Schematic set-up of the FM-DGV technique for measuring one velocity component (f_c : laser centre frequency, f_D Doppler frequency, c_L light velocity)

It is important to remark, that the Doppler frequency shift is directly proportional to the velocity component along the bisecting line of the laser incident direction and the observation direction (see the Doppler frequency f_D in fig. 3). Hence, three

different laser incident (or observation) directions are required for three component measurements.

For this reason, the three illumination directions \vec{i}_1, \vec{i}_2 and \vec{i}_3 were operated sequentially as is depicted in fig. 4. The laser light was always guided perpendicular through the transparent cover plate (made of 30 mm thick acrylic glass) and then deflected 90 deg by mirrors to reach the measurement plane, which is at the middle of the tip gap. To avoid influence on the flow field, the mirrors were installed at the outer passages (outside of upper and lower profile in fig. 4) whereby the measurements were conducted at the center blade. Qualitative flow investigations with a yarn probe proved that these mirrors have no significant influence to the investigated flow field.

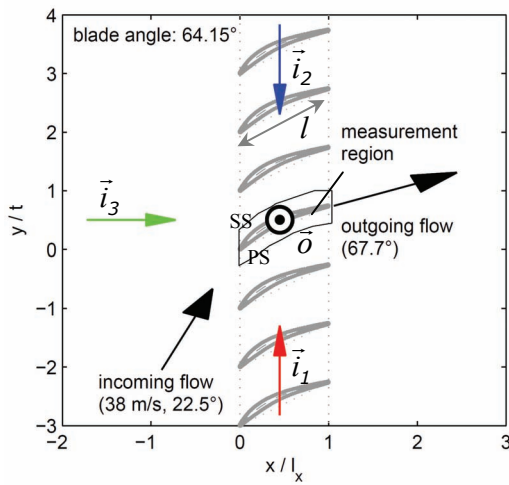


Figure 4. FM-DGV measurement arrangement in the linear cascade using three illumination directions $\vec{i}_1, \vec{i}_2, \vec{i}_3$ and one observation direction \vec{o} for three component measurements

The observation direction \vec{o} always remained the same being perpendicular to the cover plate of the cascade tunnel, which means that the scattered light was observed from outside the cascade tunnel through the acrylic glass cover plate. The FM-DGV system has 25 measurement channels [27], that are 25 fiber-coupled avalanche photo diodes, arranged in linear array configuration for maximizing the laser intensity and maximizing the scattered light power enabling low measurement uncertainties. The spatial resolution of one measurement point is about 1 mm [27].

The incident laser power in the measurement volume was about 35 mW. The FM-DGV light source is a distributed feedback diode laser with narrow linewidth (< 3 MHz) emitting at 852 nm. A fast laser frequency modulation with 100 kHz is achieved by modulating the laser diode current. The laser center frequency is stabilized to the molecular resonance frequency of cesium gas at 852 nm as is explained in [25]. Consequently, a molecular absorption cell filled with cesium gas is used for the required frequency-to-intensity conversion of the scattered light (see fig. 3). The laser and the detector unit were traversed for

measuring the field in and around the tip clearance of the center blade (see fig. 4). At each position, two subsequent acquisition cycles with a measurement duration of 1 s each were conducted. Actually, the memory of the data acquisition system allows measurements for 8 s at a stretch yielding a frequency resolution of 0.125 Hz. However, since a frequency resolution of 1 Hz was considered to be sufficient here (see section 3.1), a measurement duration of 1 s was chosen. In order to merge the measurement results of all three velocity components, the measured velocity field of each component was resampled applying linear interpolation. As a result, all three components are available at equal measurement points.

The measurement uncertainty σ_v (standard deviation of stochastic errors) depends on the scattered light power P_s (typically here about 0.5 nW) and the temporal resolution T (averaging time). As a result of signal independent noise sources such as thermal noise and in addition shot noise occurring during photo detection, the measurement uncertainty can be estimated by

$$\sigma_v = \frac{1}{\sqrt{T/s}} \cdot \sqrt{\frac{(0.0084 \text{ m/s})^2}{(P_s/nW)^2} + \frac{(0.0051 \text{ m/s})^2}{P_s/nW}}. \quad (3)$$

The underlying theory of this relation is described in [28]. The numerical values were obtained from measurements at a calibration object.

Assuming a temporal resolution $T = 1$ ms (corresponding to 1 kHz measurement rate) and a scattered light power $P_s = 0.5$ nW, the velocity uncertainty σ_v amounts to 0.58 m/s for instance. The temporal resolution (which is the reciprocal of the measurement rate here) can be adjusted by setting the averaging time. The maximum temporal resolution equals the period of one frequency modulation cycle, which is currently 10 μ s.

As a result, if sufficient tracer particles are available, high measurement rates up to 100 kHz can be achieved allowing the acquisition of turbulence spectra [27, 29]. Since this requires a high seeding concentration, tiny liquid particles of DEHS with about 1 μ m diameter were introduced locally into the incoming flow through a hole at the top of the inlet in front of plane (0) (cp. fig. 2). The particle generation rate of the particle generator with 14 Laskin nozzles amounts to $14 \cdot 10^8$ particles per second. The exact particle concentration is not known, because the seeded air is mixed with non-seeded air and, thus, the seeding concentration becomes lower downwards the flow. However, measurement rates up to about 10 kHz were achieved in the front section of the measurement region.

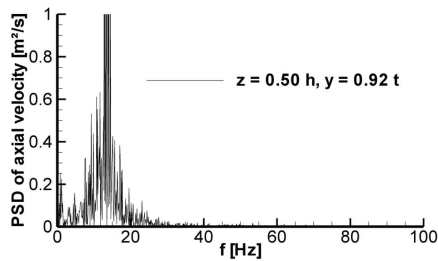
3 RESULTS AND DISCUSSION

The investigated cascade configuration is characterized by a high blade loading due to an increased incidence and turning. At this off design operation a high profile total pressure loss of about 60 % occurs (compared to 2 % at design point). To approach the account for that significant declined cascade flow first, the flow pattern measurements upstream and downstream the cascade are described followed by the discussion of the analysis of the tip clearance flow.

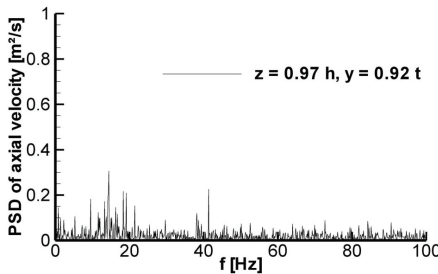
3.1 Inflow conditions and outlet flow pattern

Steady state pressure measurements $0.3 \cdot l$ upstream the cascade showed a homogenous inflow distribution with an averaged inflow angle $\alpha_1 = 22.53$ deg compared to 44 deg at the design point of the blading. The averaged velocity $c = 41$ m/s results in an estimated “virtual” inflow boundary layer thickness of $7.5 \cdot s$ related to tip clearance height caused by large blockage zones inside the cascade.

With the unsteady flow analysis by means of HWA a typical spectrum of the axial velocity component was found which is shown in fig. 5. A dominating frequency of 13 Hz appears around midspan of the blades (fig. 5a). This peak is increasingly damped inside the boundary layer until it completely disappeared $0.03 \cdot h$ off the wall (fig. 5b). Since the investigation of the inlet conditions upstream of the measuring plane did not indicate any incoming disturbances why the source of the oscillating flow behavior has to be the cascade itself.



a)



b)

Figure 5. Power Spectrum Density (one-sided) of inflow axial velocity at a) midspan and b) near the endwall (HWA Data acquired at $0.3 \cdot l$ in front of cascade)

Further analysis of the temporal velocity signal showed also a variation of the mean value of about 1-2 m/s, when the data is averaged over a period of 2 s. This is of interest when discussing the FM-DGV results in section 3.2.

The steady state wake measurements taken $0.05 \cdot l$ behind the trailing edge provide the data shown in fig. 6 for the axial velocity c_x and the outflow angle α_2 . This close axial distance does not allow intensive mixing out processes and a significant alteration of the cascade flow pattern. Hence, these data are appropriate to verify the spatial flow field idea based on the FM-DGV data inside the cascade

The averaged outflow angle α_2 defers to 67.7 deg compared to 74 deg at design point. At the upper boundary of the travers-

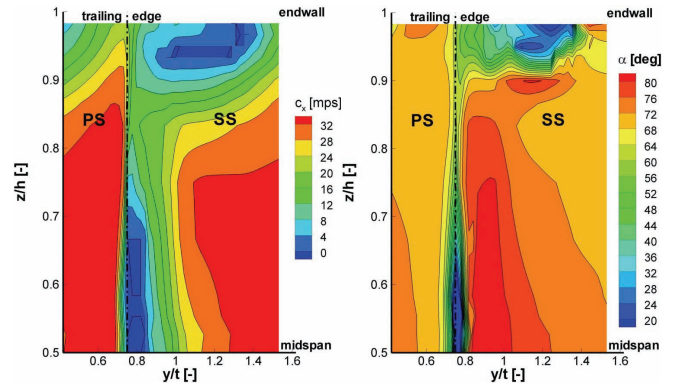


Figure 6. Outlet steady state local axial velocity and flow angle distribution (upstream view, 5HP Data acquired at $0.05 \cdot l$ behind the cascade)

ing area at $z = 0.98 \cdot h$ (comparable with the FM-DGV measurement plane) the angle differs between 75 deg in the passage and 30 deg inside the high loss area near the SS. The axial velocity plot shows a strong separation and therefore a large blockage zone at the SS around midspan. It can be clearly seen, that the tip leakage flow reduces this separation towards the endwall up to $0.2 \cdot h$ off the wall. This “energizing effect” to the separated boundary layer in the blade tip corner was found in several publications i. e. [30, 31], particularly for such high loss configurations at higher loading conditions, i. e. [32].

The high loss area in the TCV core (see fig. 7) extends up to $0.9 \cdot h$ with a pitchwise extension of $0.5 \cdot t$ near the SS. The blockage regions of adjacent passages caused by the leakage flow begin to combine near the endwall.

An evaluation of the streamwise vorticity behind the blading in fig. 7 shows massive activity in the separated SS profile boundary layer with a maximum value of about -18,000. Compared with that, the TCV mixing area between $0.92 \cdot t$ and $1.42 \cdot t$ has a more chaotic character with not clearly identifiable discrete vortex cores. This is a result of the high energy leakage jet which injects into the high turbulent separated profile flow.

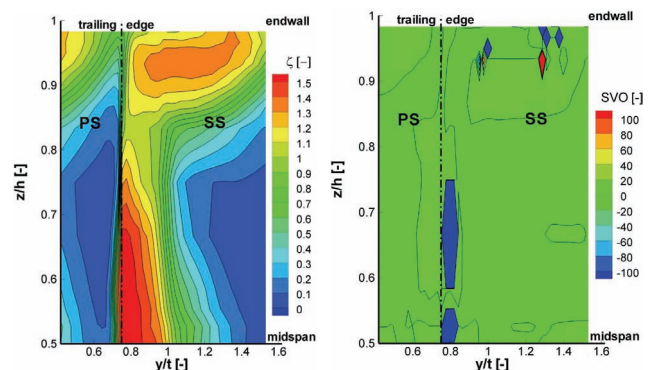


Figure 7. Total pressure loss and streamwise vorticity distribution at outlet (upstream view, 5HP Data acquired at $0.05 \cdot l$ behind the cascade)

In order to identify the turbulent activity of this area the RMS values of the axial velocity taken by the HWA are shown in fig. 8 (left). Again, like the streamwise vorticity the RMS values reach the highest magnitude of about 12 m/s in the separated profile boundary layer near the midspan. Contrarily, the area of the TCV core near the endwall shows the lowest oscillations where the highest values are much lower than at the profile separation. Surely, this is caused by the very low mean values of the axial velocity in the inside of the vortex core.

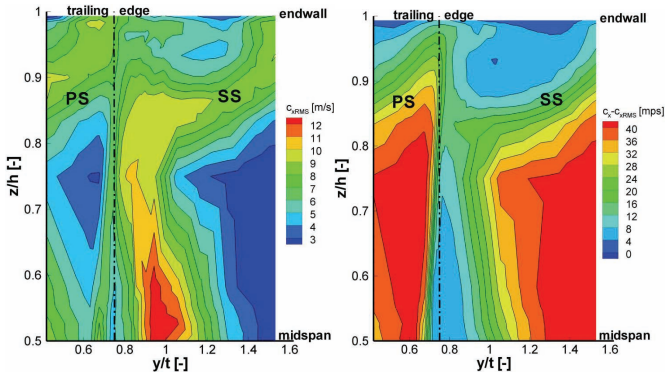


Figure 8. RMS values of the local axial velocity and subtraction from mean values (upstream view, HWA Data acquired at 0.05 / behind the cascade)

A method to find possible reversed flow in that region near the endwall caused by the TCV interaction (i. e. a “vortex spillover”, compare [33]) is to subtract the RMS values from the mean value of the axial velocity. However, in the present configuration the illustration in fig. 8 (right) does not show an outstanding area with values near 0. The only regions that nearly fulfill this condition are the separated zones of the profile and the TCV mixing area. There, the mean values are of the same magnitude like the RMS values. The lowest value of about -0.3 m/s occurred near the endwall where the probe insertion leads to additional measurement errors.

It should be remarked that the non periodicity, especially visible in the velocity plots, is caused by a small pitchwise velocity gradient at the cascade inlet plane due to the high inflow angle and the finite cascade dimensions. It is tolerated in the present work as this does not affect the qualitative TCV development and flow interaction in the occurring Re range.

The axial velocity spectra in fig. 9 were determined at characteristic points of the flow pattern. At midspan (fig. 9a), a connection between the wake of the blades (black) and the passage flow (red) far away from the surface occurs: A massive oscillation of the axial velocity with a frequency of approx. 13 Hz was found. From that it can be assumed that the profile separation pulsates with this rate. Due to the related large blockage zone around the separation the oscillation impacts the whole cascade flow. The dominating frequency is even detectable in the not effected area in the free passage, of course with much lower amplitudes in the PSD spectra. The distribution and the different amplitudes of the passage curve

also demonstrate that the wake plot peak is not caused by the inflow pattern but by the separation itself.

When considering a channel height which is cutting the vortex core at $0.93 \cdot h$, the distributions in fig. 9b can be obtained at two characteristic pitchwise positions. The passage flow outside the TCV (black) oscillates with the found dominating frequency of the profile separation.

Interestingly, the vortex core (red) does not show this behaviour. The pronounced peak decreases when traversing into the vortex until it is nearly disappeared in the vortex core. The high momentum tip leakage flow (high blade loading) damps the oscillating character in that region. The uprolling vortex does not pulsate with the passage flow around it. From the recorded data it can be assumed that the transient behaviour of the TCV is not affected by the dominating characteristic inside the cascade. Also the expected dominating frequency of approx. 200 Hz caused by the interaction of the adjacent TCV [3] could not be detected. The resulting phenomenon of an unsteady reversed axial velocity in the tip region, which was also justified in a comparable cascade [15], was not found here probably due to the much higher incidence and the outstanding profile separation.

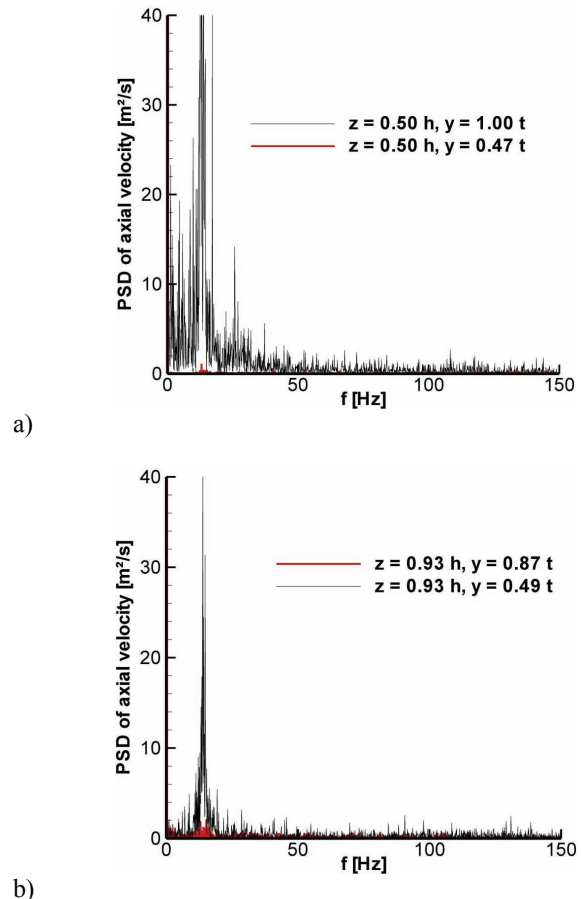


Figure 9. Power Spectrum Density (one-sided) of outlet axial velocity at a) midspan and b) near the endwall (HWA Data acquired at 0.05 / behind the cascade)

Furthermore, due to the high turbulence and therefore the high noise level the estimated blade wake shedding frequency of approx. 4 kHz could not be verified in the outlet velocity spectra. A coupling with the profile separation frequency seems to be unlikely because of the much different amplitude scales.

3.2 Passage and Tip Clearance Flow

Steady state profile pressure distribution

The conventional measuring techniques data is completed by the profile pressure distributions shown in fig. 10. Here, the vanes surface pressure is referred to the inlet plane measurements. The typical characteristic for highly loaded profiles due to high incidences was found at midspan. The highest loaded blade area is the first 10 % of chord. From there, the decreasing pressure gradient along the SS indicates separated flow caused by the large pressure gradient in front. An exact zero gradient which is characteristic for profile separation was not found due to the oscillating separation behavior along the surface in chordwise direction. From the shown pressure distribution the profile separation point can be estimated to 40 % chord.

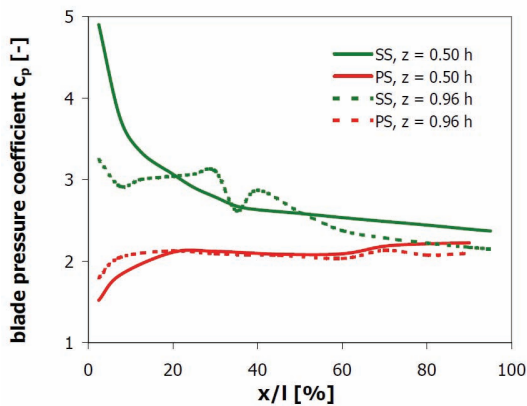


Figure 10. Steady state profile pressure distributions (pressure tappings on blade surface)

Towards the tip clearance, the TCV interaction with the profile boundary layer is detected first at the last blade height at $0.96 \cdot h$. Yet, the next pressure distribution towards midspan at $0.94 \cdot h$ does not show this clearly altered distribution compared to that at midspan. From these data, the estimated radial dimension of the TCV interaction up to $0.9 \cdot h$ from the wake measurements behind the cascade can not be verified inside the passage.

Mean velocity field

Regarding the FM-DGV measurement results, the velocity mean values are evaluated at first. The averaging is done over 2 s and the average scattered light power amounted to 0.5 nW, so that according eq. (3) the measurement uncertainty equals approximately 0.013 m/s of each measured velocity component. Hence, the stochastic errors of the velocity mean values are

negligibly small, because the velocity values are in the order of several or several ten meters per second.

The merged velocity mean values after a coordinate transform are shown in fig. 11. The velocity z -component c_z is color-coded. It clearly indicates that c_z is directed upwards into the gap at the PS and downwards to the passage at the SS. Due to the uprolling TCV, the flow is also turned upwards at the rear part of the SS. Despite the high incidence of the inflow, the cascade flow continues along the passage formed by the profiles, shown by the in-plane velocity components. This applies notably at the PS whilst the forming TCV deviates the SS flow. The measured outflow angle α_2 is approximately 75 deg at the PS and decreases to minimum 35 deg at the SS. This is in very good agreement with the results of the 5HP measurements presented in section 3.1 (see fig. 6).

With assistance of the FM-DGV measurements (see fig. 11) the dimensions of the TCV inside the clearance can be estimated by negative values of c_z . The spanwise massflow at SS is caused by the uprolling leakage jet. In axial directions the origin seems to be at $0.05 \cdot l - 0.1 \cdot l$ and the end of the vortex core at $0.9 \cdot l$. Despite of the high incidence, the pitchwise position is near the SS with the highest intensity at $0.45 \cdot l$.

With respect to the measuring uncertainty, another phenomenon shall be mentioned that was detected at the present configuration. It was found by the yarn probes at the inlet, that stochastic velocity fluctuations in pitchwise direction at the tip region occurred, as well as in the passage flow mentioned above. With time scales between 3 and 10 s they are a result of the chosen cascade configuration. The fluctuations could not be found by the HWA measurements with 35 s measurement time. A potential connection with the profile separation is ambiguous and content of further investigations. Hence, the assumption of a stationary flow is not fulfilled and can lead to measurement errors here.

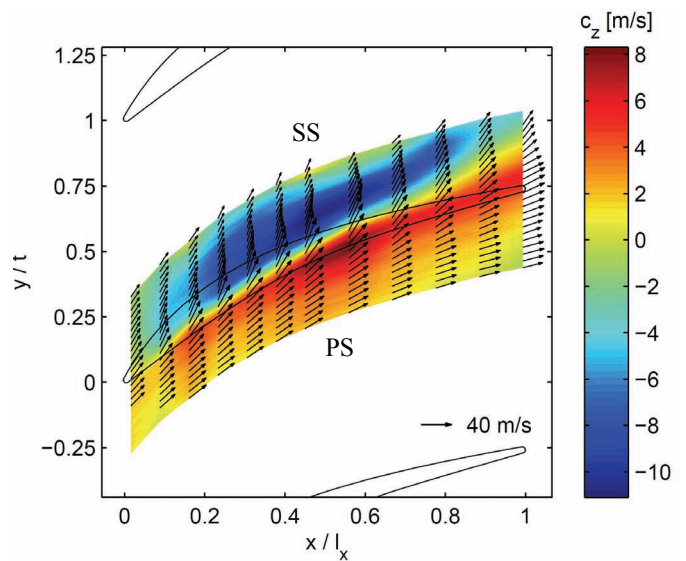


Figure 11. Mean velocity field of all three components of the tip leakage flow

Velocity standard deviation

Due to the high temporal resolution of the measurement, the velocity standard deviations could be measured also. Setting a temporal resolution of 1 ms (corresponding to a measurement rate of 1 kHz), the standard deviations σ_1 , σ_2 and σ_3 of the three measured velocity components as shown in fig. 12a, 12b and 12c are obtained. Because the measurement time for each measurement point was 2 s, the standard deviation of one measurement point is calculated from 2000 velocity values. Since the different components were measured sequentially, a coordinate transform is not possible. In x,y,z coordinates (see fig. 4), the three components are directed towards $(0,-1,1)$, $(0,1,1)$ and $(-1,0,1)$ (cp. section 2.2).

According to eq. (3), the measurement uncertainty is estimated to 0.6 m/s. Comparing with the results in fig. 11, the estimated value is smaller than the measured velocity standard deviation, which is due to the flow turbulence.

Generally, the measured flow turbulence is lower at the PS than at the SS, which holds for all velocity components. Regarding σ_1 , the flow turbulence increases sharply in the middle of the left half of the tip clearance. Furthermore, two maxima occur indicated by the arrows A_1 and A_2 . The global maximum A_1 of about 7 m/s exists at the tail of the TCV. This clearly indicates the turbulence generation of the TCV.

Concerning σ_2 , the flow turbulence structure is less significant. However, the highest flow turbulence of about 4.5 m/s occurs again in the region of the tail of the TCV indicated by the arrow B_1 . The structure at the arrow B_2 is an artifact due to a bad signal-to-noise ratio there.

When σ_3 is considered, the flow turbulence on the left of the pressure side (arrow C_2) appears to be less homogeneous than the other velocity components and is higher than on the right. On the one hand, the achieved scattered light powers is low (about 0.25 nW), so that the measurement uncertainty is increased. On the other hand, so far unknown flow phenomena can be the reason of it. However, the maximum turbulence is again at the tail of the TCV at the position C_1 .

Altogether, the turbulence in the tip leakage flow is significantly produced by the TCV. This shows the importance of a detailed understanding of the TCV, when designing new efficient compressors.

Velocity spectra

Finally, the velocity spectra inside the clearance are discussed, which can be calculated from the velocity time series simply by a harmonic analysis, because the FM-DGV system provides continuous measurements with temporally equidistant samples. This calculation method is exact for high seeding concentrations, when at least one seeding particle is present in the measurement volume of a measurement point (neglecting spatial averaging effects). Otherwise, the measurement principle is similar to a slotting technique commonly used with LDA incorporating the random arrival times of seeding particles. The considered velocity spectra were calculated from a 1 s long measurement and a chosen temporal

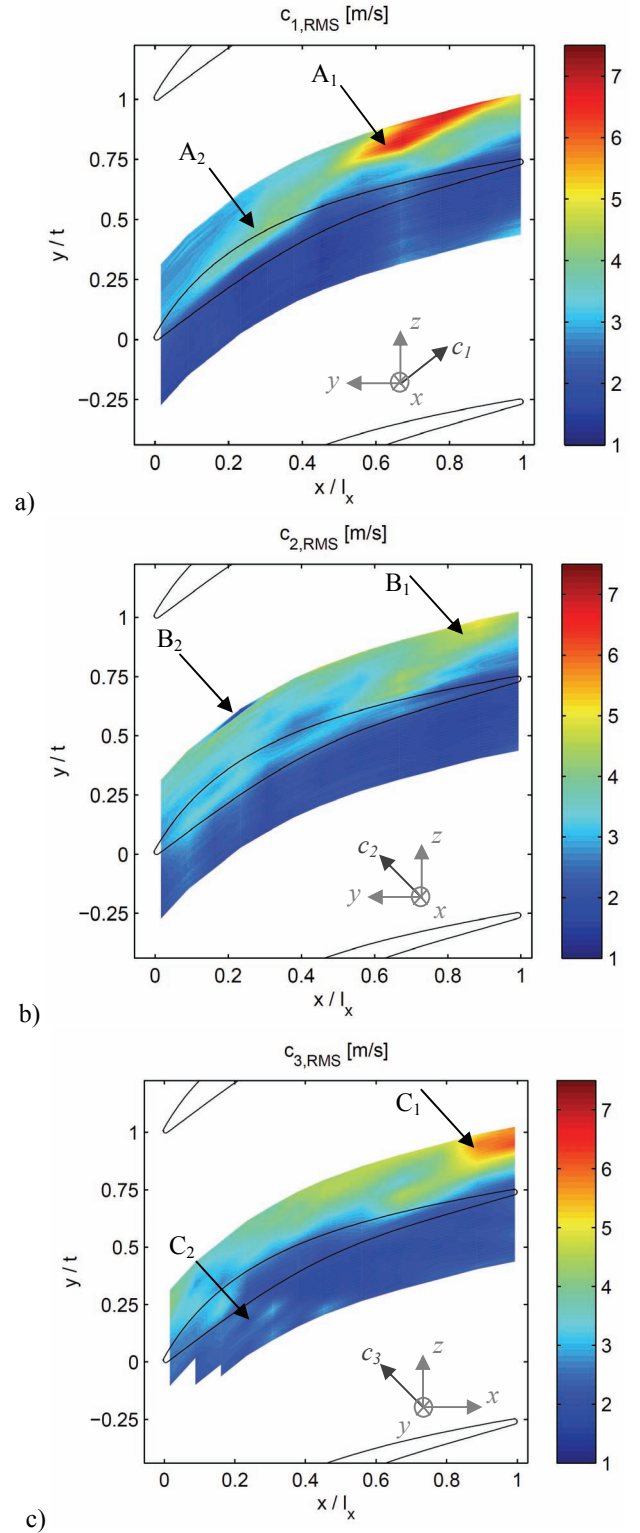


Figure 12. Velocity standard deviations σ_1 , σ_2 , σ_3 of the three measured velocity components c_1 , c_2 , c_3 along $(\vec{o} - \vec{i}_1)$, $(\vec{o} - \vec{i}_2)$, $(\vec{o} - \vec{i}_3)$ in the tip leakage flow (cp. fig. 4)

resolution of 0.5 ms (corresponding to a measurement rate of 2 kHz) yielding 2000 velocity values, a Nyquist frequency of 1 kHz and a frequency resolution of 1 Hz.

As an example, the PSD of the velocity from two positions of the first velocity component are presented in fig. 13. The first position at $x = 0.56 \cdot l_x$, $y = 0.526 \cdot t$ is located in the center of the tip clearance, whereas the second position at $x = 0.56 \cdot l_x$, $y = 0.738 \cdot t$ is at the tail of the TCV. From eq. (3), the noise power spectral density of the shown one-sided PSDs can be derived by dividing the standard deviation squared through the Nyquist frequency, which yields here about $0.7 \cdot 10^{-3} \text{ m}^2/\text{s}$. This estimated noise level coincides well with the measurement results, because the spectra converge towards approximately $2 \cdot 10^{-3} \text{ m}^2/\text{s}$ for high frequencies. Regarding the position in the tip clearance (fig. 13a), the velocity component shows almost no oscillations. At the second position in the tail of the TCV (fig. 13b), faster flow oscillations up to about 500 Hz occur. Generally, a low-pass characteristic is apparent in the spectra near the TCV, which means the oscillation amplitude is decreasing with increasing frequency. A dominating mode occurring permanently in subsequent spectra could not be detected.

As a result, the measured flow velocity spectra revealed detailed information about the flow turbulence.

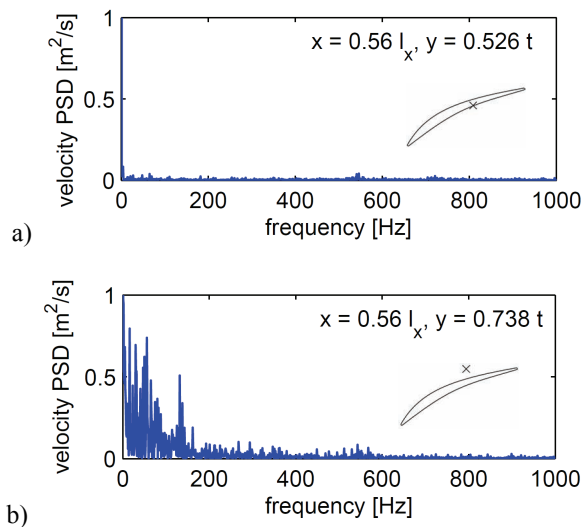


Figure 13. Velocity power spectral density (PSD, one-sided) of the first measured velocity component at two sample positions a) in the tip clearance, b) in the tail of the TCV

4 CONCLUSIONS

This article describes the application of a new optical measuring technique (Doppler global velocimetry with laser frequency modulation: FM-DGV) to a tip clearance flow in a linear compressor cascade. Supported by conventional hot-wire anemometry and pressure probes the unsteady flow pattern and the interaction between the clearance vortex and the passage

flow was determined at a high loading operating point and a clearance level of 5.2 % chord. From that experimental campaign the following conclusions can be drawn:

- This off-design operating point of the vanes near the stability limit is characterized by a 15 deg higher turning and a strong flow separation at the suction side near the trailing edge even at midspan. Additionally, a large blockage zone near the tip endwall was found caused by the TCV and its interaction with the passage flow.
- The separation and the wake total pressure losses are reduced by the leakage flow near the endwall. This decreasing impact extends up to 20 % blade height.
- Transient analysis showed the massive profile separation to be the dominating unsteady effect in the wake of the cascade with an axial velocity oscillating frequency of about 13 Hz. Due to the high blockage of this separation the complete passage flow pulsates with the same frequency. This effect is even detectable at the inflow and is damped towards the endwall.
- The tip clearance vortex constitutes the dominating flow effect near the endwall and generates turbulence. The highest turbulence intensity was measured at the tail of the vortex.
- Investigating the measured velocity spectra in the tip clearance zone, no dominant oscillation frequency could be determined. The turbulence appears to be mainly chaotic with low frequency parts having higher amplitudes than the high frequency parts. Therefore the tip clearance vortex seems not to interact with the oscillating passage flow in its unsteady behavior.
- The expected dominating frequency of approx. 200 Hz for the interaction of adjacent tip clearance vortices as well as a vortex spillover were not detected. The applied near stall conditions and the resulting profile flow impeded the development of the mentioned phenomena.

Finally the applied FM-DGV technique was proven to be a valuable tool for the turbulence analysis of a complex, three dimensional flow in turbomachines. In addition to its demonstrated capability for measuring time-varying flow effects, two-point correlations can be also evaluated in future. Furthermore, the presented planar measurement can be conducted for multiple planes at different heights. This will provide investigations of the three-dimensional structure of a tip clearance flow.

ACKNOWLEDGMENTS

The financial support of the Deutsche Forschungsgemeinschaft (DFG) for the project Cz55/22-1 is gratefully acknowledged.

REFERENCES

- [1] Wisler, D.C., 1985: „Loss Reduction in Axial Flow Compressors Through Low-Speed Model Testing”, ASME Journal of Turbomachinery, Vol. 107, pp. 354-363
- [2] Hoying, D. A., Tan, C.S., Vo, H.D., Greitzer, E.M., 1998: „Role of Blade Passage Flow Structures in Axial Compressor Rotating Stall Inception”, ASME Paper No. 98-GT-588
- [3] Mailach, R., Lehmann, I., Vogeler, K., 2001: „Rotating Instabilities in an Axial Compressor Originating from the Fluctuating Blade Tip Vortex”, ASME Journal of Turbomachinery, Vol. 123, pp. 453-463
- [4] Vo, D.H., Tan, C.S., Greitzer, E.M., 2005: „Criteria for Spike Initiated Rotating Stall”, ASME Paper No. GT-2005-68374
- [5] Chen, G. T., Greitzer, E. M., Tan, C. S., Marble, F. E., 1991: „Similarity Analysis of Compressor Tip Clearance Flow Structure”, ASME Journal of Turbomachinery, Vol. 113, pp. 260-271
- [6] Storer, J.A., and Cumpsty, N.A., 1991: „Tip Leakage Flow in Axial Compressors”, ASME Journal of Turbomachinery, Vol. 113, pp. 252-259
- [7] Lakshminarayana, B., Zaccaria, M., Marathe, B., 1995: „The Structure of Tip Clearance Flow in Axial Flow Compressors”, ASME Journal of Turbomachinery, Vol. 117, pp. 336-347
- [8] Tan, C.S., 2006: „Three-Dimensional and Tip Clearance Flows in Compressors”, Von Kármán Institute for Fluid Dynamics (VKI), Lecture Series 2006-06 “Advances in Axial Compressor Aerodynamics”, Rhode-Saint-Genèse, Belgium, May 15-18, 2006
- [9] M. Sell, M. Treiber, C. Casciaro, G. Gyarmathy, 1999: „Tip-clearance-affected flow fields in a turbine blade row”, Proceedings of the Institution of Mechanical Engineers, Part A, 213:309 – 318
- [10] Murthy, K.N.S., Lakshminarayana, B., 1986: „Laser Doppler Velocimeter Measurements in the Tip Region of a Compressor Rotor”, AIAA Journal, Vol. 24, pp. 807-814
- [11] Stauter, R.C., Dring, R.P., Carta, F.O., 1991: „Temporally and Spatially Resolved Flow in a Two-Stage Axial Compressor: Part I - Experiment”, ASME Journal of Turbomachinery, Vol. 113, pp. 212-226
- [12] Hathaway, M.D., Suder, K.L., Okiishi, T.H., Strazisar, A.J., Adamczyk, J.J., 1987: „Measurement of the Unsteady Flow Field Within the Stator Row of a Transonic Axial-Flow Fan: Part II – Results and Discussion”, ASME Paper No. 87-GT-227
- [13] Lehmann, I., Wolf, E., Vogeler, K., 2001: „Stator Wake Propagation Inside Rotating Blade Passages”, ImechE C557/006/99, Proceedings of the 4th European Conference on Turbomachinery, Florence, Italy
- [14] Mailach, R., Lehmann, I., and Vogeler, K., 2008: „Periodical Unsteady Flow Within a Rotor Blade Row of an Axial Compressor: Part I: Flow Field at Midspan. Part II: Wake - Tip Clearance Vortex Interaction”, ASME Journal of Turbomachinery, Vol. 130, pp. 041004-1 - 041004-10, 041005-1 - 041005-10.
- [15] Mailach, R., 2001: „Experimentelle Untersuchung von Strömungsinstabilitäten im Betriebsbereich zwischen Auslegungspunkt und Stabilitätsgrenze eines vierstufigen Niedergeschwindigkeits-Axialverdichters”, doctoral thesis, TU Dresden; also published as: Fortschritt-Berichte VDI, Reihe 7, Nr. 410, VDI-Verlag, Düsseldorf, Germany.
- [16] Suder, K.L., Celestina, M.L., 1994: „Experimental and Computational Investigation of the Tip Clearance Flow in a Transonic Axial Compressor Rotor”, ASME Paper No. 94-GT-365
- [17] Michon, G.-J., Miton, H., and Ouayahya, N., 2005: „Unsteady Off-Design Velocity and Reynolds Stresses in an Axial Compressor”, AIAA Journal of Propulsion and Power, Vol. 21, No. 6, pp. 961-972
- [18] Ma, H., Jiang, H., Zhang, Q., 2001: „Three-Dimensional Unsteady Flow Field due to IGV-Rotor Interaction in the Tip Region of an Axial Compressor Rotor Passage”, ASME Paper No. 2001-GT-0296
- [19] Tisserant, D., Breugelmans, F.A.E., 1997: „Rotor Blade-to-Blade Measurements Using Particle Image Velocimetry”, ASME Journal of Turbomachinery, Vol. 119, pp. 176-181
- [20] Balzani, N., Scarano, F., Riethmüller, M.L., Breugelmans, F.A.E., 2000: „Experimental Investigation of the Blade-to-Blade Flow in a Compressor Rotor by Digital Particle Image Velocimetry”, ASME Journal of Turbomachinery, Vol. 122, pp. 743-750
- [21] Sanders, A.J., Papalia, J., Fleeter, S., 2001: „Multi-Blade Row Interactions in a Transonic Axial Compressor, Part I: Stator Particle Image Velocimetry (PIV) Investigations”, ASME Paper No. 2001-GT-0268
- [22] Liu, B., Wang, H., Liu, H., Yu, H., Jiang, H., and Chen, M., 2004: „Experimental Investigation of Unsteady Flow Field in the Tip Region of an Axial Compressor Rotor Passage at Near Stall Condition With Stereoscopic Particle Image Velocimetry”, ASME Journal of Turbomachinery, Vol. 126, pp. 360-374.
- [23] M. Voges, C. Willert, R. Mönig, M. W. Müller, H.-P. Schiffer, 2010: „The challenge of stereo PIV measurements in the tip gap of a transonic compressor rotor with casing treatment”, 15th International Symposium on Applications of Laser Techniques to Fluid Mechanics, No. 1.9.2 (11 p.), Lisbon
- [24] M. P. Wernet, D. Van Zante, T. J. Strazisar, W. T. John, P. S. Prah, 2005: „Characterization of the tip clearance flow in an axial compressor using 3-D digital PIV”, Experiments in Fluids 39: 743 – 753
- [25] Fischer, A., Büttner, L., Czarske, J., Eggert, M., Grosche, G., Müller, H., 2007: „Investigation of time-resolved single detector Doppler global velocimetry using sinusoidal laser frequency modulation”, Meas. Sci. Tech. 18: 2529 – 2545
- [26] Fischer, A., Büttner, L., Czarske, J., Eggert, M., Müller, H., 2009: „Measurements of velocity spectra using time-resolving Doppler global velocimetry with laser frequency modulation and a detector array”, Exp. Fluids 47: 599–611
- [27] Fischer, A., Büttner, L., Czarske, J., Eggert, M., Müller, H., 2009: „Array Doppler Global Velocimeter with Laser Frequency Modulation for Turbulent Flow Analysis – Sensor investigation and application”, in: Imaging Measurement Methods for Flow Analysis (Eds. W. Nitsche, C. Dobriloff), Springer, Berlin, pp. 31-41
- [28] Fischer, A., Büttner, L., Czarske, J., Eggert, M., Müller, H., 2008: „Measurement uncertainty and temporal resolution of Doppler global velocimetry using laser frequency modulation”, Applied Optics 47(21): 3941 – 3953
- [29] Fischer, A., König, J., Czarske, J., 2008: „Speckle noise influence on measuring turbulence spectra using time-resolved Doppler global velocimetry with laser frequency modulation”, Meas. Sci. Tech. 19: 125402 (15 p.)
- [30] Lakshminarayana, B., 1970: „Methods of predicting the tip clearance effects in axial flow turbomachinery”, ASME Journal of Basic Engineering, 92(1):467–482
- [31] Williams, R., Gregory-Smith, D., He, L., Ingram, G., 2010: „Experiments and computations on large tip clearance effects in a linear cascade”, ASME Journal of Turbomachinery, 132(2):18–21.
- [32] Clemen, C., Gümmer, V., Nerger, D., Saathoff, H., 2007: „Investigation of different endwall part-clearance configurations on a low speed compressor cascade”, 7th European Turbomachinery Conference, Athens, Greece.
- [33] Saathoff, H., Stark, U., 1999: „Endwall boundary layer separation in a single-stage axial-flow low-speed compressor and a high-stagger compressor cascade”, Forschung im Ingenieurwesen, Vol. 65, pp. 217-224